



Microresonator soliton frequency combs via cascaded Brillouin scattering



Hao Zhang ^{1,2,6}, Shuangyou Zhang ^{1,3,6}, Toby Bi ^{1,4}, George Ghalanos¹, Yaojing Zhang ^{1,5}, Haochen Yan ^{1,4}, Arghadeep Pal^{1,4}, Jijun He ²✉, Shilong Pan ²✉ & Pascal Del'Haye ^{1,4}✉

Microresonator frequency combs are vital for advancing optical communications and sensing, but current methods face challenges in achieving low phase noise and flexible repetition rates simultaneously. Here, we demonstrate forward-propagating soliton frequency combs using cascaded Brillouin scattering in a silica resonator. This method bridges distinct resonator modes and decouples soliton repetition rates from the Brillouin frequency shift (~10 GHz in silica). By generating soliton pulses at 107 GHz, we show that the repetition rates can be tailored through resonator geometry without compromising low noise. This integration of Brillouin lasing with microcombs unites stability and design flexibility, overcoming prior limitations. The results can enable scalable photonic platforms for applications such as LiDAR, high-capacity optical networks, and precision microwave generation. This technique is of interest for technologies that demand both ultra-stable and customizable light sources.

Dissipative Kerr solitons (DKS) that rely on the Kerr nonlinearity within high-Q microresonators have received significant research interest because of their potential use in a large number of photonic applications. Soliton frequency combs have, in particular, garnered attention for their small footprint and small power consumption for out-of-the-lab applications^{1–7}. Leveraging advanced fabrication techniques across diverse optical platforms, creating DKS with repetition rates spanning from several GHz to several THz has become possible. Attainable frequency ranges cover the microwave, millimeter-wave, and terahertz domains, leading to potential applications like ultra-fast ranging^{8–10}, dual-comb spectroscopy^{11,12}, high-speed optical communications¹³, photonic signal generation^{14,15}, and astro-combs^{16,17}.

Significant progress has been made in DKS generation in recent years, particularly through the interaction between a stimulated Brillouin laser (SBL)^{18,19} and the nonlinear Kerr effect. This innovative approach has been demonstrated across multiple platforms, such as fiber Fabry–Pérot (FFP) cavities^{20,21}, silica microdisk resonators²² and silica wedge resonators²³, silica microsphere²⁴, silica microtoroid²⁵. In this concept, a pump laser generates a Brillouin sideband, which in turn generates a Kerr soliton frequency comb. This is an intriguing approach because the pump laser can remain on the thermally stable blue-detuned side of a microresonator mode. An alternative approach for stable soliton generation by balancing thermal effects has been

shown by employing dual pumping using an auxiliary laser^{26,27}. This configuration achieves self-stabilization for thermal compensation and ensures the robust generation of solitons²⁸. Dual pumping has enabled comb generation with improved phase noise, comb linewidth, and timing jitter²¹ compared to earlier DKS schemes.

First-order Brillouin scattering and, thus also, the generated soliton combs are backward propagating with respect to the pump laser. To the best of our knowledge, there is no report of SBL-Kerr soliton generation based on higher-order stimulated Brillouin scattering, which can be co-propagating with the pump light. Here, we introduce an implementation of dissipative Kerr solitons that are generated by a cascaded process of forward-propagating stimulated Brillouin scattering (SBS) within a fused silica rod^{29,30}. The experiments are done in resonators with a free spectral range (FSR) of 107 GHz, which is not linked to the SBS frequency shift. Our results establish the feasibility of achieving SBS-cascaded Kerr solitons with arbitrary repetition rates conducted by exciting different-order Brillouin laser sidebands. These findings could be interesting for optical communication, ranging, and photonic microwave generation in integrated photonic platforms.

Results

Figure 1a shows the theoretical concept of the forward SBS cascaded comb generation. If the Brillouin gain overlaps with a resonator mode and

¹Max Planck Institute for the Science of Light, 91058 Erlangen, Germany. ²National Key Laboratory of Microwave Photonics, Nanjing University of Aeronautics and Astronautics, Nanjing, 210016, China. ³Department of Electrical and Photonics Engineering, Technical University of Denmark, Kgs, Lyngby, 2800, Denmark.

⁴Department of Physics, Friedrich Alexander University Erlangen-Nuremberg, 91058 Erlangen, Germany. ⁵School of Science and Engineering, The Chinese University of Hong Kong, Shenzhen, Guangdong, 518172, China. ⁶These authors contributed equally: Hao Zhang, Shuangyou Zhang.

✉ e-mail: jjun.he@nuaa.edu.cn; pans@nuaa.edu.cn; pascal.delhaye@mpl.mpg.de

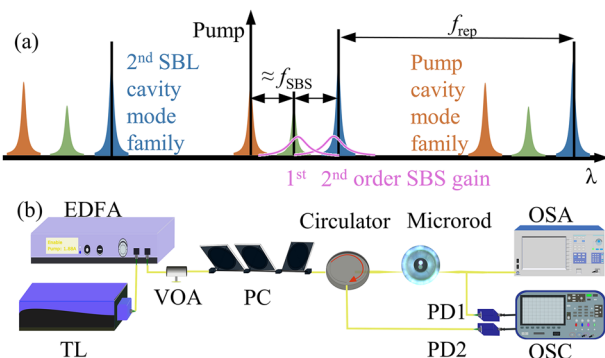


Fig. 1 | Schematic and experimental setup for Brillouin soliton frequency comb generation. **a** Schematic diagram of the cascaded Brillouin scattering (SBS) and comb generation process. The orange resonances represent the pump cavity mode family, the green resonances correspond to the mode family for the 1st-order SBS sidebands, and the cyan resonances show the mode family that overlaps with the 2nd-order SBS sideband. The pink solid curves represent the 1st-order and 2nd-order stimulated Brillouin lasing (SBL) gain regions excited by the pump laser. f_{rep} : Brillouin frequency shift. f_{rep} : the repetition rate of the comb. **b** Experimental setup for the forward SBS cascaded soliton generation. TL tunable laser, EDFA erbium-doped fiber amplifier, VOA variable optical attenuator, PC polarization controller, PD photodiode, OSA optical spectrum analyzer, OSC oscilloscope.

surpasses the cavity losses, it undergoes strong amplification and becomes the dominant lasing mode. In our case, both the 1st and 2nd-order SBS gain regions overlap with cavity modes, giving rise to 2nd-order cascaded SBS. The generated SBS sidebands can give rise to four-wave mixing (FWM) induced optical frequency combs. By controlling the pump laser detuning, the SBS sideband starts to generate a low noise dissipative Kerr soliton.

To realize the proposed method, we set up the experiment shown in Fig. 1b. An external tunable laser with power and polarization control is used as the pump source. This laser is directed toward a 0.3-mm-radius silica microrod cavity^{29,30} with many higher-order mode families. Many of the modes in the different mode families have a frequency offset that matches the SBS gain offset. The oscilloscope (OSC) captures the signals of both the forward and backward propagation from the microrod cavity with two photodetectors (PDs). In addition, these signals can be recorded using an optical spectrum analyzer (OSA).

As shown in Fig. 2a, we observe forward-propagating soliton states. The blue solid line is a fitted sech^2 envelope, which closely matches the measured spectrum. Zooming into the spectrum, as depicted in Fig. 2b, the measured FSR is around 0.87 nm (107 GHz). The spacing between the pump cavity mode and the neighboring cavity mode for the 1st SBS sideband is 0.09 nm. Note that the first-order SBS sideband is backwards propagating in the microresonators. Thus, the measured signal in a forward direction in Fig. 2b only shows a weak signal for the first-order SBS sideband, which originates from backscattering within the resonator. The spacing between the pump cavity mode and the 2nd SBL cavity mode utilized for generating the SBL-Kerr soliton is 0.18 nm. This mode spacing matches the frequency shift for the 2nd-order stimulated Brillouin sideband of 22.5 GHz. Note that the signal measured with the OSA has been attenuated by a 10-dB optical attenuator and optical couplers.

Figure 2c, d shows forward transmission spectra of the microrod cavity at low and high optical pump power. The inset of Fig. 2d provides a close-up of the transmission of the cavity mode that overlaps with the 2nd-order SBL gain³¹. Details on the dispersion of the 3 mode families can be found in Figure S2 of the Supplemental Material. The different mode families for the pump laser, 1st and 2nd order Brillouin sidebands are marked with colored circles. Moreover, the measured linewidths of the pump mode, the mode of the 1st SBS sideband, and the mode of the 2nd SBS sideband are 13.3, 3.99, and 1.6 MHz (see Fig. 2e), whereas their corresponding loaded quality (Q) factors are 1.4×10^7 , 4.8×10^7 and 1.2×10^8 , respectively.

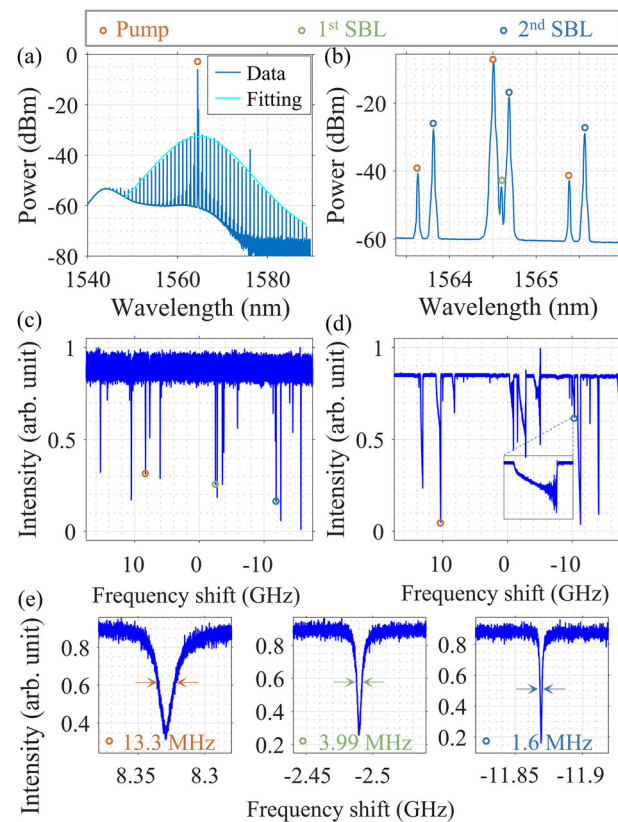


Fig. 2 | Optical spectra of forward-propagating Brillouin solitons and mode spectra of the microresonator. **a** Measured spectrum of a forward propagating single soliton. The cyan-colored solid line is a sech^2 fit. **b** Close-up of the spectrum of (a). The different mode families for the pump laser, 1st and 2nd order Brillouin sidebands are marked with colored circles, according to the legend on top. **c** Forward transmission spectrum of the microrod cavity at low optical pump power. **d** Forward transmission spectrum at high optical pump power. The inset is a close-up of the 2nd-order stimulated Brillouin laser (SBL) cavity mode. **e** Linewidth of the pump mode (13.3 MHz), the 1st SBL cavity mode (3.99 MHz), and the 2nd SBL cavity mode (1.6 MHz).

In order to study the SBL-Kerr interactions, we scan the tunable pump laser across the pump mode with a power of 15 dBm. The corresponding transmission and reflection curves are shown in Fig. 3. In contrast to a uniform conventional thermal triangle, we can divide the transmission/reflection curves into three parts.

In region I, the intracavity buildup is less than the threshold power for the SBS and parametric oscillations. Consequently, only the pump laser without sidebands is measured on the OSA in this region (see Fig. 4a). When red-detuning the laser frequency, the overlap between the SBL gain region and the SBS cavity mode increases. Once this overlap is sufficiently strong, the backward propagating 1st-order SBS sideband is excited together with a forward propagating 2nd-order SBS sideband, which can be seen as region II in Fig. 3. Initially, the backward intensity substantially increases due to the 1st-order SBS process. When passing through region II, the overlap of the 2nd order SBS gain region and its corresponding cavity mode increases, which leads to a reduction in backward propagating light. Consequently, in Region II, we can observe simultaneously the pump laser, the 1st-order Brillouin lasing, and the 2nd-order Brillouin lasing on the optical spectrum analyzer (see Fig. 4b).

Since the measured loaded Q factor of the 2nd-order SBS cavity mode (1.2×10^8) is much higher than that of the pump mode (1.4×10^7), the effective loaded Q factor in the forward direction becomes better when more intracavity power is transferred to the 2nd-order SBS cavity mode in region II.

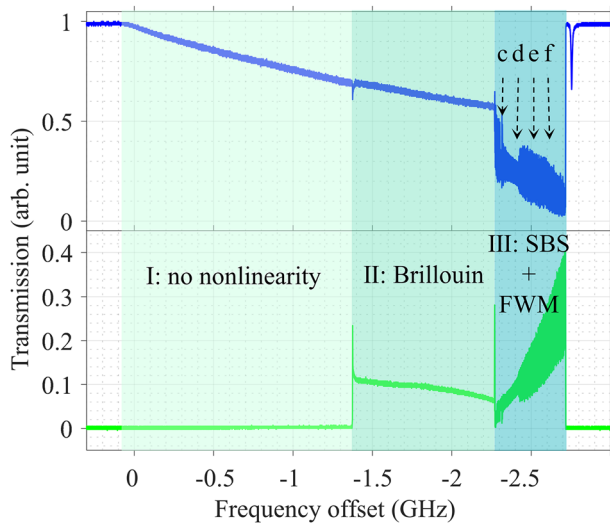


Fig. 3 | Cavity dynamics as a function of laser detuning. Transmission (blue) and reflection (green) of the microresonator mode when scanning the pump laser from high to low frequencies. We observe three distinct regions in the thermally broadened resonance (I, II, III). Four different comb states can be accessed and are marked with dashed arrows: c = modulational instability comb, d = single soliton, e = multi-solitons, f = perfect soliton crystal. SBS stimulated Brillouin Scattering, FWM four-wave mixing.

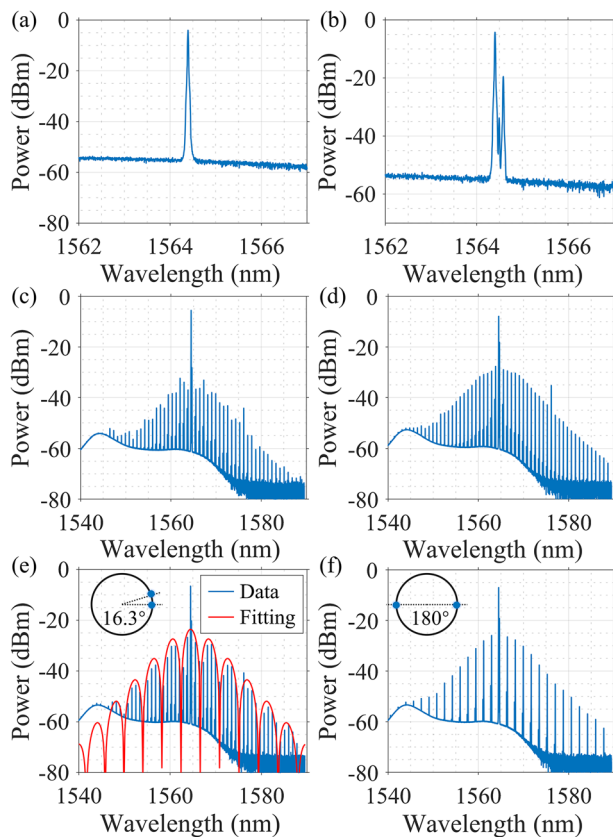


Fig. 4 | Comb generation dynamics. Optical spectra of (a) pump laser without nonlinearity, (b) Brillouin scattering, (c) stimulated Brillouin scattering (SBS) assisted modulational instability comb, (d) SBS-assisted single soliton, (e) multi-solitons, (f) perfect 2-free spectral range (FSR) soliton crystal. The red line fits the measurement data, revealing that the multi-soliton state corresponds to two solitons with an angular offset of 16.3° within the resonator.

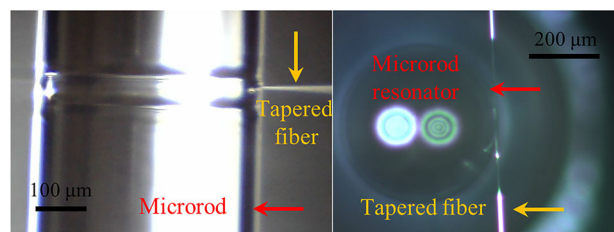


Fig. 5 | Microscopy images of the microresonator. Front view (left) and top view (right) of the microrod used in our experiments. The microrod resonator is marked by the red arrow, while the tapered fiber is marked by the yellow arrow.

When we further red-detune the laser frequency, we enter region III. Here, parametric oscillations induced directly from the 2nd-order Brillouin lasing appear and create multiple optical sidebands. In addition, the pump laser itself generates optical sidebands through four-wave mixing. This can be seen as a chaotic modulational instability comb in Fig. 4c. After traversing this chaotic region, we reach the soliton region, starting with a single soliton shown in Fig. 4d, a multi-soliton state shown in Fig. 4e, and eventually, a perfect soliton crystal shown in Fig. 4f. These soliton combs are centered around the second order SBS sideband. The faintly visible Turing pattern comb in the background of the OSA spectra is directly generated by the pump light and is spectrally offset from the soliton combs. For further characterization of the multi-soliton state in Fig. 4e, we added a fit to the measurement data. This fit reveals that the multi-soliton state corresponds to two solitons with an angular offset of 16.3° within the resonator. The soliton states remain stable for several hours during our experiments. Since the exact soliton number for the bright soliton is not predetermined, a multi-soliton is typically observed upon entering the soliton region. However, we can deterministically reduce the number of solitons by using the backward-detuning method described in Ref. 32, to obtain a single soliton state. Note that in previous work, the presence of cascaded Brillouin scattering prevented the generation of dissipative Kerr solitons^{20,33}. Here we show, that both processes can coexist within a microresonator. Additional data for the SBS-induced solitons are in the supplementary material, including reconfigurability (Fig. S1), dispersion measurement (Fig. S2) properties in the backward direction (Fig. S3), repetition rate difference (Fig. S4), and theoretical analysis (Fig. S5) with simulation parameters (Table S1).

Conclusion

In summary, we demonstrate a mechanism to generate forward propagating solitons that are induced by cascaded Brillouin scattering. Our work presents stable soliton states with a repetition rate of 107 GHz using a fused silica microrod resonator. Leveraging the abundance of different mode families within the microrod cavity, we can overlap the SBS gain regions with cavity modes to support the cascaded soliton generation process. Moreover, our findings introduce an approach for generating soliton combs in cavities with a large number of co-existing mode families. The soliton generation happens in a different mode family, which leads to a repetition rate that is independent of the Brillouin frequency shift. Thus, this method has the potential to generate SBL-induced soliton combs at arbitrary repetition rates by using microresonators with different diameters. In future work, SBS-assisted comb generation could also be implemented in planar multimode resonators or in planar resonators with sidewall modulation-induced mode splitting³⁴. Our approach allows us to achieve low-noise solitons via low-noise Brillouin lasing, which is essential for photonic signal generation³⁵ and optical atomic clock devices^{36,37}. Moreover, SBL-induced soliton combs can have applications in optical communication, ranging, and photonic microwave generation.

Methods

The fused silica microresonator is fabricated by CO₂-laser lathe machining of fused-quartz rods. With this method, the microresonator diameters can be in the range between ~150 μm and 8 mm (FSR between 440 GHz and 8 GHz). The microresonator used in our manuscript exhibits anomalous dispersion with an FSR of 107 GHz with loaded quality factors exceeding 10⁸. The front view and top view of the microrod used in our experiments are shown in Fig. 5. We use a tapered fiber to evanescently couple light into the microresonator. The coupling rate can be optimized by adjusting the diameter of the tapered fiber and its position relative to the fused silica microresonator. The coupling condition can be reproduced reasonably well with a closed-loop piezo positioning system.

Data availability

Data sets generated during the current study are available from the corresponding author upon reasonable request.

Received: 29 October 2024; Accepted: 10 April 2025;

Published online: 24 May 2025

References

1. Kippenberg, T. J., Gaeta, A. L., Lipson, M. & Gorodetsky, M. L. Dissipative Kerr solitons in optical microresonators. *Science* **361**, eaan8083 (2018).
2. Gaeta, A. L., Lipson, M. & Kippenberg, T. J. Photonic-chip-based frequency combs. *Nat. Photonics* **13**, 158–169 (2019).
3. Jang, Y. S. et al. Nanometric precision distance metrology via hybrid spectrally resolved and homodyne interferometry in a single soliton frequency microcomb. *Phys. Rev. Lett.* **126**, 023903 (2021).
4. Chang, L., Liu, S. & Bowers, J. E. Integrated optical frequency comb technologies. *Nat. Photonics* **16**, 95–108 (2022).
5. Bruch, A. W. et al. Pockels soliton microcomb. *Nat. Photonics* **15**, 21–27 (2020).
6. Bao, H. et al. Laser cavity-soliton microcombs. *Nat. Photonics* **13**, 384–389 (2019).
7. Shen, B. et al. Integrated turnkey soliton microcombs. *Nature* **582**, 365–369 (2020).
8. Suh, M.-G. & Vahala, K. J. Soliton microcomb range measurement. *Science* **359**, 884–887 (2018).
9. Trocha, P. et al. Ultrafast optical ranging using microresonator soliton frequency combs. *Science* **359**, 887–891 (2018).
10. Riemensberger, J. et al. Massively parallel coherent laser ranging using a soliton microcomb. *Nature* **581**, 164–170 (2020).
11. Bernhardt, B. et al. Cavity-enhanced dual-comb spectroscopy. *Nat. Photonics* **4**, 55–57 (2009).
12. Yang, Q. F. et al. Vernier spectrometer using counterpropagating soliton microcombs. *Science* **363**, 965–968 (2019).
13. Lundberg, L. et al. Phase-coherent lightwave communications with frequency combs. *Nat. Commun.* **11**, 201 (2020).
14. Liu, J. et al. Photonic microwave generation in the X- and K-band using integrated soliton microcombs. *Nat. Photonics* **14**, 486–491 (2020).
15. Zhang, S. et al. Terahertz wave generation using a soliton microcomb. *Opt. Express* **27**, 35257–35266 (2019).
16. Obrzud, E. et al. A microphotonic astrocomb. *Nat. Photonics* **13**, 31–35 (2018).
17. Suh, M. G. et al. Searching for exoplanets using a microresonator astrocomb. *Nat. Photonics* **13**, 25–30 (2019).
18. Asano, M. et al. Stimulated Brillouin scattering and Brillouin-coupled four-wave-mixing in a silica microbottle resonator. *Opt. Express* **24**, 12082–12092 (2016).
19. Wang, H., Lai, Y. H., Yuan, Z., Suh, M. G. & Vahala, K. Petermann-factor sensitivity limit near an exceptional point in a Brillouin ring laser gyroscope. *Nat. Commun.* **11**, 1610 (2020).
20. Jia, K. et al. Photonic flywheel in a monolithic fiber resonator. *Phys. Rev. Lett.* **125**, 143902 (2020).
21. Nie, M. et al. Synthesized spatiotemporal mode-locking and photonic flywheel in multimode mesoresonators. *Nat. Commun.* **13**, 6395 (2022).
22. Bai, Y. et al. Brillouin-Kerr soliton frequency combs in an optical microresonator. *Phys. Rev. Lett.* **126**, 063901 (2021).
23. Do, I. H. et al. Self-stabilized soliton generation in a microresonator through mode-pulled Brillouin lasing. *Opt. Lett.* **46**, 1772–1775 (2021).
24. Zhang, H. et al. Soliton microcombs multiplexing using intracavity-stimulated Brillouin lasers. *Phys. Rev. Lett.* **130**, 153802 (2023).
25. Zhang, M. et al. Strong interactions between solitons and background light in Brillouin-Kerr microcombs. *Nat. Commun.* **15**, 1661 (2024).
26. Zhang, S., Silver, J. M., Bi, T. & Del'Haye, P. Spectral extension and synchronization of microcombs in a single microresonator. *Nat. Commun.* **11**, 6384 (2020).
27. Strekalov, D. V. & Yu, N. Generation of optical combs in a whispering gallery mode resonator from a bichromatic pump. *Phys. Rev. A* **79**, 041805 (2009).
28. Zhang, S. et al. Sub-milliwatt-level microresonator solitons with extended access range using an auxiliary laser. *Optica* **6**, 206–212 (2019).
29. Del'Haye, P., Diddams, S. A. & Papp, S. B. Laser-machined ultra-high-Q microrod resonators for nonlinear optics. *Appl. Phys. Lett.* **102**, 221119 (2013).
30. Svela, A. O. et al. Coherent suppression of backscattering in optical microresonators. *Light Sci. Appl.* **9**, 204 (2020).
31. Zhang, S., Bi, T. & Del'Haye, P. On-the-fly precision spectroscopy with a dual-modulated tunable diode laser and Hz-level referencing to a cavity. *Adv. Photonics* **6**, 046003 (2024).
32. Guo, H. et al. Universal dynamics and deterministic switching of dissipative Kerr solitons in optical microresonators. *Nat. Phys.* **13**, 94–102 (2016).
33. Braje, D., Hollberg, L. & Diddams, S. Brillouin-enhanced hyperparametric generation of an optical frequency comb in a monolithic highly nonlinear fiber cavity pumped by a CW laser. *Phys. Rev. Lett.* **102**, 193902 (2009).
34. Lu, X., Rogers, S., Jiang, W. C. & Lin, Q. Selective engineering of cavity resonance for frequency matching in optical parametric processes. *Appl. Phys. Lett.* **105**, 151104 (2014).
35. Xie, X. et al. Photonic microwave signals with zeptosecond-level absolute timing noise. *Nat. Photonics* **11**, 44–47 (2016).
36. Papp, S. B. et al. Microresonator frequency comb optical clock. *Optica* **1**, 10–14 (2014).
37. Newman, Z. L. et al. Architecture for the photonic integration of an optical atomic clock. *Optica* **6**, 680–685 (2019).

Acknowledgements

National Natural Science Foundation of China (62205145); National Key Research and Development Program of China (2022YFB2802700); Natural Science Foundation of Jiangsu Province (BK20220887); China Scholarship Council (202106830063); European Union's H2020 ERC Starting Grant "CounterLight" (756966); H2020 Marie Skłodowska-Curie COFUND "Multiply" (713694); Marie Curie Innovative Training Network "Microcombs" (812818); the University Development Fund (UDF01003527, The Chinese University of Hong Kong, Shenzhen).

Author contributions

H.Z. and S.Z. contributed equally to this work. H.Z. fabricated the cavity and performed the experiments. H.Z. and S.Z. designed the experiments. T.B. built the processing platform for Microrod. G.G. and A.P. built the setup for fabricating tapered fibers. H.Z. and J.H. conducted the theoretical analysis. H.Z., S.Z., T.B., Y.Z., and H.Y. analyzed the data. H.Z.

wrote the paper, with input from the other authors. P.D., J.H., and S.P. supervised the project.

Funding

Open Access funding enabled and organized by Projekt DEAL.

Competing interests

The authors declare no competing interests.

Additional information

Supplementary information The online version contains supplementary material available at <https://doi.org/10.1038/s42005-025-02095-0>.

Correspondence and requests for materials should be addressed to Jijun He, Shilong Pan or Pascal Del'Haye.

Peer review information *Communications Physics* thanks the anonymous reviewers for their contribution to the peer review of this work.

Reprints and permissions information is available at <http://www.nature.com/reprints>

Publisher's note Springer Nature remains neutral with regard to jurisdictional claims in published maps and institutional affiliations.

Open Access This article is licensed under a Creative Commons Attribution 4.0 International License, which permits use, sharing, adaptation, distribution and reproduction in any medium or format, as long as you give appropriate credit to the original author(s) and the source, provide a link to the Creative Commons licence, and indicate if changes were made. The images or other third party material in this article are included in the article's Creative Commons licence, unless indicated otherwise in a credit line to the material. If material is not included in the article's Creative Commons licence and your intended use is not permitted by statutory regulation or exceeds the permitted use, you will need to obtain permission directly from the copyright holder. To view a copy of this licence, visit <http://creativecommons.org/licenses/by/4.0/>.

© The Author(s) 2025